HHS Public Access

Author manuscript

Mol Imaging. Author manuscript; available in PMC 2015 April 06.

Published in final edited form as:

Mol Imaging. 2011 April ; 10(2): 91–101.

Nerve-Highlighting Fluorescent Contrast Agents for Image-Guided Surgery

Summer L. Gibbs-Strauss, Ph.D.[1], **Khaled Nasr, Ph.D.**[1], **Kenneth M. Fish, Ph.D.**[2], **Onkar Khullar, M.D.**[3], **Yoshitomo Ashitate, M.D.**[1], **Tiberiu M. Siclovan, Ph.D.**[2], **Bruce F. Johnson, Ph.D**[2], **Nicole E. Barnhardt, B.S.**[2], **Cristina A. Tan Hehir, Ph.D.**[2], and **John V. Frangioni, M.D., Ph.D.**[1,4,*]

[1]Division of Hematology/Oncology, Beth Israel Deaconess Medical Center, Boston, MA 02215

[2]Molecular Imaging and Diagnostic Advanced Technology Program, GE Global Research, Niskayuna, NY 12309

[3]Division of Thoracic Surgery, Brigham and Women's Hospital, Boston, MA 02215

[4]Department of Radiology, Beth Israel Deaconess Medical Center, Boston, MA 02215

Abstract

Nerve damage is the major morbidity of many surgeries, resulting in chronic pain, loss of function, or both. The sparing of nerves during surgical procedures is a vexing problem because surrounding tissue often obscures them. To date, systemically administered nerve-highlighting contrast agents that can be used for nerve-sparing image-guided surgery have not been reported. In the current study, physicochemical and optical properties of 4,4'-[(2-methoxy-1,4-phenylene)di-(1E)-2,1-ethenediyl]bis-benzenamine (BMB) and a newly synthesized, red-shifted derivative 4-[(1E)-2-[4-[(1E)-2-[4-aminophenyl]ethenyl]-3-methoxyphenyl]ethenyl]-benzonitrile (GE3082) were characterized *in vitro* and *in vivo*. Both agents crossed the blood-nerve barrier and blood-brain barrier, and rendered myelinated nerves fluorescent after a single systemic injection. Although both BMB and GE3082 also exhibited significant uptake in white adipose tissue, GE3082 underwent a hypsochromic shift in adipose tissue that provided a means to eliminate the unwanted signal using hyperspectral deconvolution. Dose and kinetic studies were performed in mice to determine the optimal dose and drug-imaging interval. Results were confirmed in rat and pig, with the latter used to demonstrate, for the first time, simultaneous fluorescence imaging of blood vessels and nerves during surgery using the FLARE™ (Fluorescence-Assisted Resection and Exploration) imaging system. These results lay the foundation for the development of ideal nerve-highlighting fluorophores for image-guided surgery.

Keywords

Nerve-highlighting contrast agents; fluorescence; blood-nerve barrier; image-guided surgery; FLARE™ imaging system

* To whom all correspondence should be addressed: John V. Frangioni, M.D., Ph.D. BIDMC, Room SL-B05 330 Brookline Avenue Boston, MA 02215 617-667-0692 FAX: 617-667-0981 jfrangio@bidmc.harvard.edu.

INTRODUCTION

Surgery is among the most commonly recommended treatments for major acute and chronic diseases, with as many as 40 million procedures conducted each year in the U.S. alone [1]. A common, but under-recognized clinical complication of these procedures following healing of the surgical site is chronic pain from nerve damage, with an estimated 0.05 to 1.5% prevalence up to one year post-surgery [1]. Though the incidence is low, the absolute number is quite large, ranging from 20,000 to 600,000 patients per year. Persistent post-surgical pain, formally recognized approximately 10 years ago [2-4], is now termed “chronic post-surgical pain” or “post-surgical neuralgia.” In fact, nerve damage is a major morbidity associated with many surgical procedures, including inguinal hernia repair [5, 6], lumpectomy and mastectomy [7-9], thoracic surgery [10, 11], coronary artery bypass [12, 13] and prostatectomy [14, 15]. In spite of the knowledge base of human nerve anatomy, surgery that spares the nervous structures is still a difficult task due to patient-to-patient variability and the difficulty of nerve visualization. Nerves are usually protected deep within the tissue, rendering them difficult to detect prior to injury from surgical dissection. Damage to nerves during surgery often leads to chronic pain, loss of function, or both [1, 4, 15, 16].

Much of the difficulty with chronic pain and loss of function can be attributed to the fact that currently, most surgical procedures are performed without the assistance of image-guidance. Although ultrasound and x-ray fluoroscopy are used selectively during human surgery [17], the former requires direct contact with tissue and sees only a narrow slice within the surgical field, and the latter exposes patients and caregivers to ionizing radiation. More importantly, neither technique is amenable to low doses of targeted contrast agents and are, thereby, unable to provide nerve-specific imaging.

Optical imaging has tremendous clinical potential for image-guided surgery. Through administration of exogenous contrast agents specific for nervous tissues, the nerve anatomy could be directly visualized in real-time during surgery. The use of near-infrared (NIR) wavelengths between 700 to 900 nm is particularly attractive for nerve-specific contrast agents because tissue autofluorescence, absorbance, and scatter are minimal in this region of the electromagnetic spectrum [18, 19]. Importantly, NIR fluorescent contrast agents can now be visualized during surgery using the FLARE™ (Fluorescence-Assisted Resection and Exploration) intraoperative imaging system [20-24], which is currently being used in three NIH- funded clinical trials [25]. While developing agents with desirable characteristics is a challenge, a nerve-specific fluorescent contrast agent would be of immediate benefit to patients and surgeons for image-guidance during numerous surgical procedures.

The ideal nerve-specific contrast agent should fulfill the following criteria: 1) have a LogD at pH 7.4 between 0.5 to 3 to maximize blood-nerve barrier (BNB) penetration [26, 27], 2) have a molecular weight ≤ 500 Da to maximize BNB penetration [26, 27], 3) bind to a nerve-specific target and be retained in the nervous tissue for several hours, and 4) have excitation and emission maximum wavelengths in the NIR region of the electromagnetic spectrum. The current study focused on characterizing the utility of a previously described nerve-specific contrast agent, 4,4’-[(2-methoxy-1,4-phenylene)di-(1E)-2,1-ethenediyl]bis-benzenamine (BMB) [28] and a red-shifted derivative of this molecule, 4-[(1E)-2-[4-

[(1E)-2-[4-aminophenyl]ethenyl]-3-methoxyphenyl]ethenyl]-benzonitrile (GE3082) (Nasr, *et al*., manuscript in preparation), for image-guided surgery. The goals of this study were to fully characterize the physicochemical and optical properties of these fluorophores *in vitro* and *in vivo*, define an effective formulation for intravenous (IV) administration, characterize the dose effect and kinetics of both fluorophores, and demonstrate their performance during image-guided surgery in mice, rats and pigs.

MATERIALS AND METHODS

Synthesis of Nerve-Highlighting Contrast Agents BMB and GE3082

The nerve-specific fluorescent contrast agents 4,4'-[(2-methoxy-1,4-phenylene)di-(1E)-2,1-ethenediyl]bisbenzenamine (BMB; Figure 1A) and 4-[(1E)-2-[4-[(1E)-2-[4-aminophenyl]ethenyl]-3-methoxyphenyl]ethenyl]-benzonitrile (GE3082; Figure 1B) were synthesized using a modified Horner-Wittig olefination (Nasr, *et al*., manuscript in preparation).

Physicochemical Characterization of BMB and GE3082

Absorbance and fluorescence spectra of 10 μM solutions of BMB and GE3082 were measured in dimethyl sulfoxide (DMSO), absolute methanol (MeOH), fetal bovine serum (FBS) buffered with 20 mM HEPES, and the formulation used for IV administration (10% DMSO, 5% Cremophor, 65% serum, and 20% HEPES buffer; IV Formulation) using fiber-optic HR2000 (200-1100 nm) and USB2000FL (350-1000 nm) spectrometers (Ocean Optics, Dunedin, FL), respectively. Fluorescence excitation was provided by a 375 ± 10 nm light emitting diode (LED). The extinction coefficients of BMB and GE3082 were calculated at the excitation maximum in DMSO, MeOH, FBS and the IV Formulation. The quantum yields of BMB and GE3082 in DMSO, MeOH, FBS, and the IV Formulation were measured by comparing the integrated fluorescence emission of the fluorophores in each solvent to the emission of 7-Ethylamino-6-methyl-4-trifluormethylcoumarin (a.k.a., Coumarin 503, Coumarin 307; Exciton, Dayton, OH) in MeOH (quantum yield = 15% [29, 30]) as a reference standard under conditions of matched absorbance at the excitation wavelength. The LogD values of BMB and GE3082 at pH 7.4 were calculated using Marvin JChem Software (Budapest, Hungary).

Animals

All animals used in this study were studied under the supervision of an approved institutional protocol. CD-1 mice of either sex weighing 28 g to 30 g and Sprague-Dawley rats of either sex weighing 225 g to 250 g were purchased from Charles River Laboratories (Wilmington, MA). Male Yorkshire pigs weighing 30 kg were purchased from E. M. Parsons & Sons (Hadley, MA). Prior to surgery, mice and rats were anesthetized with 65 mg/kg intraperitoneal (IP) pentobarbital (Ovation Pharmaceutical, Inc., Deerfield, IL). Pig anesthesia was induced with 4.4 mg/kg intramuscular Telazol® (Fort Dodge Animal Health, Fort Dodge, IA), and maintained with 2% isoflurane after intubation.

Intraoperative Fluorescence Imaging

The FLARE™ intraoperative imaging system has been described in detail previously [20-24], and its use for nerve-specific imaging is explained briefly as follows. For excitation two 375 ± 10 nm LEDs (Epitex, Inc., Kyoto, Japan) fitted with 370 nm short pass (SP) filters were used, which created a fluence rate of 0.15 mW/cm^2 on the imaging field. All filters and beam splitters were from Chroma Technology, Brattleboro, VT. To image the emission of BMB a 550 ± 25 nm filter was used. To image the emission of GE3082 a 610 ± 38 nm filter was used. Fluorescence images were collected using exposure times ranging from 67 to 500 msec. All images collected for comparison between vehicle-injected control animals and fluorophore-injected animals had the same exposure time and normalization. Color video images were collected on a separate channel using custom designed optics and software.

Simultaneous nerve and vessel fluorescence imaging was performed using GE3082 for nerve contrast and indocyanine green (ICG) for vessel contrast. The same excitation and emission wavelengths mentioned previously were used for GE3082 fluorescence imaging. ICG was excited using 760 ± 30 nm LEDs (Epitex) fitted with 764 ± 17 nm filters in custom holders that produced a fluence rate on the imaging field of 8.5 mW/cm^2. To image the emission of ICG an 824 ± 24 nm filter was used.

Formulation, Dosing and Kinetics for *In Vivo* Fluorescence Imaging

The lipophilic nature of BMB and GE3082 required specialized formulation for IV administration. Formulations containing 1 – 10% DMSO, 1 – 5% Cremophor and 0 – 65% serum were tested by centrifugation for 5 minutes at 10,000 g. Formulations in which the fluorophores remained completely in solution following centrifugation were composed of 10% DMSO, 5% Cremophor, 65% serum and 20% HEPES buffer at pH 7.4. This “IV Formulation” was used for all subsequent IV administrations.

Dose and kinetic experiments were performed in mice where the brachial plexus nerve was exposed and imaged over a 4 h period. The brachial plexus nerve to surrounding muscle tissue ratio was calculated. The doses of BMB and GE3082 were serially decreased from 0.5 mg/mouse to 0.03125 mg/mouse. Control mice were administered IV Formulation only (vehicle). Images of the mouse brachial plexus region were acquired using the FLARE™ intraoperative imaging system prior to fluorophore administration, 5, 10, 15, 30, 45 and 60 min after administration and then every 30 min for 4 h following fluorophore administration. Three mice were evaluated for each fluorophore at each dose over the 4 h period.

In Vivo Optical Spectroscopy

BMB and GE3082 were evaluated in mice by imaging their trigeminal ganglia with a Maestro™ small animal multi-spectral imaging system (CRI, Woburn, MA). Four h after IV administration of the 0.25 mg/mouse dose of the fluorophore in the IV Formulation, the mice were sacrificed, and their trigeminal ganglia, optic nerves and brain were exposed for imaging. A 390 nm short-pass (SP) filter was used for excitation; the fluorescence emission spectra were collected between 500 and 800 nm at 10 nm intervals. The trigeminal ganglia, optic nerves and brain of the vehicle-injected control animals were imaged using the same

integration time as each fluorophore-injected animal. The *in vivo* fluorescence spectra of BMB and GE3082 in the nerve, adipose and muscle tissues were unmixed from the nerve, adipose, and muscle tissues of vehicle-injected control animals using the software supplied by the manufacturer. Using the spectral signature of each tissue, representative nerve, adipose, and muscle images were unmixed from the original fluorescence image using the same manufacturer supplied software.

Nerve Imaging of Rats and Pigs

Using the dosing and kinetics information from mice, BMB and GE3082 were evaluated in rats using the 0.25 mg/mouse dose scaled by weight. Rats (225 g) were administered 2 mg of fluorophore in the IV Formulation. Four h after administration the brachial plexus, sciatic nerve, trigeminal ganglia, and optic nerves were exposed and imaged. The nerves and adipose tissues were resected for analysis by fluorescence microscopy. Both BMB and GE3082 were also evaluated in Yorkshire pigs (n = 7) where the dose was scaled by body surface area (BSA; 272-fold difference compared to mouse). BMB was administered at a BSA-equivalent of the 0.25 mg/mouse dose, or 68 mg. GE3082 was administered at a BSA-equivalent of the 0.125 mg/mouse dose, or 34 mg. Images of the brachial plexus and sciatic nerves were acquired at 4 h and 8 h following IV administration. ICG in saline, 2.5 mg per dose, was administered as an IV bolus for NIR fluorescence angiography. The nerve and adipose tissues were resected for analysis by fluorescence microscopy.

Histology and Microscopy

Tissues from mice, rats and pigs were preserved for microscopic assessment and localization of fluorescent signal. Tissues were resected from the animal and placed in 2% paraformaldehyde in PBS (pH 7.4) for 12 h before mounting in Tissue-Tek OCT compound (Fisher Scientific, Pittsburgh, PA) and flash-freezing in LN_2. Each sample was serially cryo-sectioned (10 μm per slice); one slide was stained with hematoxylin and eosin (H&E) and a consecutive section was used for fluorescence microscopy.

For *ex vivo* fluorescence microscopy, serial sections were imaged on a Nikon TE 300 microscope system equipped with a mercury excitation source (Chiu Technical Corporation, Kings Park, NY), CoolSNAP HQ^2 14-bit camera for fluorescence imaging (Photometrics, Tucson, AZ), QImaging 12-bit camera for color imaging (Surrey, BC, Canada), and iVision software (BioVision Technologies, Exton, PA), using the following excitation and emission filters combinations. To obtain fluorescence images of BMB the mercury light source was passed through a 360 ± 20 nm BP excitation filter, a 400 nm LP beam splitter, and a 550 ± 50 nm BP emission filter. To obtain fluorescence images of GE3082 the mercury light source was passed through a 360 ± 20 nm BP excitation filter, a 400 nm LP beam splitter, and a 610 ± 38 nm BP emission filter. Exposure times were adjusted between 400 and 5000 ms for fluorescence images.

RESULTS

Physiochemical and Optical Property Characterization of BMB and GE3082

BMB and GE3082 have molecular weights of 342 Da and 352 Da, and LogD values at pH 7.4 of 4.8 and 5.5, respectively. The absorbance and fluorescence spectra of BMB and GE3082 were tested in solvents with varied proton content including DMSO, MeOH, FBS, and the formulation used for IV administration (IV Formulation). Overall, GE3082 exhibited a 80- to 100-nm red shift in peak fluorescence emission compared to BMB. Whereas BMB showed very similar absorbance and fluorescence in each of the four solvents (Figure 1A), the spectral shape of GE3082 was significantly affected by solvent (Figure 1B). A dual fluorescence peak was seen in DMSO and MeOH, while a single peak was seen in FBS and the IV Formulation for GE3082. The dual fluorescence peak was more pronounced in MeOH than in DMSO. The asymmetric resonance structure of GE3082 is affected by excitation wavelength, pH, and solvent polarity. A physicochemical mechanism accounting for these complex spectral results is being published elsewhere (Nasr et al., manuscript in preparation).

The extinction coefficient of BMB was similar in DMSO, MeOH and the IV Formulation, but lower in FBS (Figure 1A). The extinction coefficient of GE3082 was highest in DMSO and MeOH, and lowest in the IV Formulation and FBS (Figure 1B). The quantum yield of BMB was moderate in DMSO and MeOH, and only two-fold lower in FBS and the IV Formulation (Figure 1A). In contrast, the quantum yield of GE3082 was one to two orders of magnitude lower in DMSO and MeOH compared to FBS and the IV Formulation (Figure 1B).

In Vivo Optical Property Characterization of BMB and GE3082

The spectral properties of BMB and GE3082 were examined *in vivo* in the mouse trigeminal ganglia, optic nerve, brain, adipose and muscle tissues. The fluorescence spectrum of BMB was similar in the nerve and adipose tissues with the emission maxima at 540 nm in both tissues. Minimal fluorescence was seen in the surrounding muscle tissue, which had an emission maximum at 550 nm (Figure 2A). In contrast, the fluorescence spectrum of GE3082 was blue-shifted in white adipose tissue (emission maximum = 560 nm) as compared to its spectrum in nervous tissues (emission maximum = 600 nm) (Figure 2B). Some GE3082 fluorescence was detected in muscle with an emission maximum of 610 nm. Using the spectral shape differences between nerve, adipose and muscle, unmixed images of each tissue were created which illustrated the contribution of each tissue to the total fluorescence signal (Figure 2).

Nerve-Specific Fluorescence *In Vivo* and *Ex Vivo*

BMB and GE3082 were found to highlight all large nervous structures in mice, rats and pigs including the brachial plexus, spine, sciatic, optic, trigeminal ganglia, facial, vagus, femoral, penile, and phrenic nerves. Example rat images of the brachial plexus, sciatic, trigeminal ganglia, and optic nerve are shown in Figure 3 for BMB (Figure 3A) and GE3082 (Figure 3B). Both BMB and GE3082 showed accumulation in the nerves and adipose tissues. The brachial plexus and trigeminal ganglia were resected and serially sectioned for analysis by

fluorescence microscopy. Both examples showed fluorescence throughout the cross-sectioned nerve (Figure 3A and 3B, bottom rows).

Dose and Kinetics of BMB and GE3082

The dose-response and kinetics of both BMB and GE3082 were studied in mice. The brachial plexus nerves were exposed by resection of the pectoralis major prior to administration of 0.03125 to 0.5 mg/mouse of BMB or GE3082. Background fluorescence was measured prior to IV administration of each fluorophore. Images of each animal were acquired over a 4-h period following BMB or GE3082 administration and post-processed using line profile analysis to determine the fluorescence maxima in the brachial plexus and surrounding muscle tissue. The fluorescence maxima were assessed in three regions of each brachial plexus nerve and surrounding muscle tissue (n = 6 sites total per animal) to reveal the average nerve-to-muscle ratio for each dose (Figure 4A and 4B). Following BMB administration, the muscle fluorescence increased rapidly over the first 15 minutes after IV administration, resulting in a nerve-to-muscle contrast of less than one. After 15 minutes, the muscle fluorescence decreased as the nerve fluorescence increased over the 4 h period, resulting in a nerve-to-muscle ratio greater than one (Figure 4A). Following GE3082 administration, nerve and muscle tissues showed similar contrast over the first 15 minutes resulting in a nerve-to-muscle ratio near one. After 15 minutes, reduction in fluorescence of the muscle and increase in fluorescence of the nerve resulted in a nerve-to-muscle ratio greater than one (Figure 4B). Both BMB and GE3082 showed maximum fluorescence at the 4 h time point (Figure 4). The linear dose range for both BMB and GE3082 was between 0.0625 mg/mouse and 0.25 mg/mouse. The lowest dose tested for both fluorophores, 0.03125 mg/mouse, did not show significant fluorescence contrast over vehicle-injected control animals and the highest dose tested, 0.5 mg/mouse, appeared to be a saturated dose as it did not show linear increase in nerve-to-muscle contrast as compared with the 0.25 mg/mouse dose. Nerve-to-muscle contrast was maintained for up to 8 h following IV administration of either fluorophore (data not shown). Nerve-to-muscle signal was maintained longer for GE3082 than for BMB where nerve-to-muscle signal was 20% of peak for GE3082 as compared to 2% of peak for BMB 24 h after IV administration (data not shown).

As might be expected due to its significant red shift in fluorescence emission, GE3082 showed higher nerve-to-muscle contrast than BMB for all tested doses at 4 h after administration (Figure 4C). This was due to increased nerve signal following GE3082 administration as compared to BMB administration, with similar muscle fluorescence for both compounds (Figure 4D). Of note, GE3082 also had significantly higher adipose tissue accumulation than BMB (Figure 4D) and thus lower nerve to adipose contrast. Adipose tissue fluorescence was maintained similar to nerve fluorescence for up to 8 h following IV administration (data not shown). Adipose to muscle signal was maintained longer for GE3082 than for BMB where adipose to muscle signal was 60% of peak for GE3082 as compared to 15% of peak for BMB 24 h after IV administration (data not shown).

Image-Guided Surgery in Pig

The dose and kinetic experiments in mice were used to scale the dose for nerve imaging in pig. Without administration of BMB, no fluorescence contrast in the nervous tissues over the muscle was seen (Figure 5, row 1). After IV administration of BMB in pig, images of the sciatic nerve and brachial plexus were collected 4 h and 8 h post-injection. Nerve-to-muscle contrast was highest 8 h after BMB administration, as can be seen in the example sciatic nerve image (Figure 5, row 2). The sciatic nerve and surrounding adipose tissue were resected and preserved for analysis by fluorescence microscopy. As seen in the rat nerves, BMB fluorescence was seen throughout the cross-sectioned nerve bundles (Figure 5, row 3). BMB also highlighted the adipose tissue, which was localized to the membranes of the lipid droplets (Figure 5, row 4).

After IV administration of GE3082 into 30 kg Yorkshire pigs, images of the sciatic nerve and brachial plexus were acquired at 4 h and 8 h. Nerve-to-muscle contrast was similar at the 4 h and 8 h time points. ICG was administered during brachial plexus imaging and enabled simultaneous nerve and vessel imaging (Figure 6A). The brachial plexus and surrounding adipose tissue were resected and preserved for microscopic analysis. Similar to the pig sciatic nerve with BMB, the brachial plexus nerve showed GE3082 fluorescence throughout the cross-sectioned nerve bundles (Figure 6B). GE3082 also showed significant fluorescence signal in the adipose tissue, although the pattern of fluorescence was different than that of BMB. GE3082 accumulated in both the membrane as well as the cytosol of the lipid droplet (Figure 6B).

DISCUSSION

With 40 million surgical procedures performed annually in the United States [1], nerve damage is inevitable. As a result, patients suffer from chronic pain as well as loss of normal bodily functions, which could possibly be avoided if the nerves could be seen prior to their injury. Nerve contrast agents that bind specifically to myelin have been used for histopathological examination of the nervous system for nearly 50 years [31-33], and more recently, additional fluorophores have been developed for rapid, selective staining of myelin in brain tissue sections [34, 35]. Contrast agents have also been developed to assess the anatomy and function of peripheral nerve tissue through intramuscular administration and retrograde transport [36]. Although myelinated nerve staining techniques are widely used for histopathology and *ex vivo* examination of tissue sections, none of these compounds can be used as *in vivo* nerve contrast agents because they are impermeable to the blood-brain barrier (BBB) and blood-nerve barrier (BNB) [34]. To date only a few select molecules have been found to penetrate the BNB and BBB, and specifically stain nervous tissues *in vivo*. These molecules fall into three main classes: 1) stilbene derivatives [37], 2) BDB ((E,E)-1,4-bis(4’-aminostyryl)-2-dimethoxy-benzene) [34] and BMB [28], and 3) the styryl pyridinium dyes (FM Dyes) [38, 39].

The most promising class of nerve staining dyes developed to date includes BMB and BDB, as well as the potential derivatives that could be synthesized from this base structure, such as GE3082. Although BMB administered IV was found to produce high nerve-to-muscle contrast, BDB was found to selectively stain only the corpus callosum and cerebellum when

applied to frozen sections or when administered IV [34], but not other nervous tissues (data not shown). BMB (Figure 1A) and GE3082 (Figure 1B) fulfill 2 of the 4 criteria for an ideal nerve-highlighting dye. BMB and GE3082 have molecular weights ≤ 500 Da and bind to a nerve-specific target, likely myelin [28], which enables retention in the nerve tissue for up to 8 hours after systemic administration. The LogD at pH 7.4 of BMB and GE3082 are above the ideal range of 0.5 to 3, rendering them more lipophilic than necessary for BBB and BNB penetration [26, 27] and helping to explain their significant accumulation in adipose tissue. Both fluorophores were studied following systemic administration and their use was demonstrated during image-guided surgery. BMB and GE3082 were found to penetrate the BBB and BNB following IV administration, and highlighted peripheral and central nervous tissues in mice, rats (Figure 3) and pigs (Figures 5 and 6). Although uptake in adipose tissue was significant for both agents, the spectral shift of GE3082 in adipose tissue permitted separation of nerve signal from those of adipose and muscle tissues (Figure 2B).

A key characteristic of fluorescent contrast agents for image-guided surgery is the use of fluorophores that absorb and emit in the NIR region (700 to 900 nm) of the electromagnetic spectrum. Indeed, red-shifting BMB emission towards the NIR was the primary motivation for synthesizing GE3082. NIR fluorescent contrast agents are significantly advantageous over agents that absorb and emit at wavelengths below 700 nm because tissue autofluorescence, absorbance, and scattering are at their minimum in the NIR wavelengths [18, 19]. The most important criterion for an ideal nerve-specific contrast agent not fulfilled by BMB and GE3082 is a fluorophore that absorbs and emits in the NIR region. Although both BMB and GE3082 theoretically have enough double bonds to resonate in the NIR, the symmetry of these molecules results in ultraviolet and visible absorption and emission. In the IV Formulation, the maximum absorbance and fluorescence of GE3082 was red-shifted 21 nm and 81 nm, respectively from BMB (Figure 1). A similar fluorescence red-shift was seen *in vivo* between GE3082 and BMB in nerve tissue, where the maximum nerve fluorescence for GE3082 was 60 nm above that of BMB (Figure 2). Ongoing studies are aimed at further modifying the base structure to promote resonance along the full length of the available conjugated π-system, while retaining nerve-specific uptake.

The base structure of BMB and GE3082 is a promising start to a nerve-specific contrast agent for image-guided surgery. Both BMB and GE3082 highlight central and peripheral nerve tissue for up to 8 hours following systemic administration. The current fluorophores could be significantly improved by decreasing the LogD at pH 7.4 into the ideal range for BBB and BNB penetration, which would likely decrease adipose tissue signal, and decreasing the resonance symmetry, to increase the wavelength of absorbance and emission. Although a significant challenge, a nerve-specific NIR fluorescent contrast agent would be of immediate benefit to both patients and surgeons for nerve-sparing image-guided surgery.

ACKNOWLEDGMENTS

We thank Lorissa Moffitt and Eugenia Trabucchi for editing and administrative assistance, and Victoria Madigan for experimental assistance. This work was funded by a Sponsored Research Agreement to the Beth Israel Deaconess Medical Center by GE Global Research.

REFERENCES

1. Burke S, Shorten GD. When pain after surgery doesn't go away. Biochem Soc Trans. 2009; 37(Pt 1):318–22. [PubMed: 19143655]
2. Crombie IK, Davies HT, Macrae WA. Cut and thrust: antecedent surgery and trauma among patients attending a chronic pain clinic. Pain. 1998; 76(1-2):167–71. [PubMed: 9696470]
3. Eisenberg E. Post-surgical neuralgia. Pain. 2004; 111(1-2):3–7. [PubMed: 15327802]
4. Macrae WA. Chronic post-surgical pain: 10 years on. Br J Anaesth. 2008; 101(1):77–86. [PubMed: 18434337]
5. Franneby U, et al. Risk factors for long-term pain after hernia surgery. Ann Surg. 2006; 244(2):212–9. [PubMed: 16858183]
6. Jenkins JT, O'Dwyer PJ. Inguinal hernias. Br Med J. 2008; 336(7638):269–72. [PubMed: 18244999]
7. Carpenter JS, et al. Risk factors for pain after mastectomy/lumpectomy. Cancer Pract. 1999; 7(2): 66–70. [PubMed: 10352063]
8. Macdonald L, et al. Long-term follow-up of breast cancer survivors with post-mastectomy pain syndrome. Br J Cancer. 2005; 92(2):225–30. [PubMed: 15655557]
9. Poleshuck EL, et al. Risk factors for chronic pain following breast cancer surgery: a prospective study. J Pain. 2006; 7(9):626–34. [PubMed: 16942948]
10. Kalso E, et al. Chronic post-sternotomy pain. Acta Anaesthesiol Scand. 2001; 45(8):935–9. [PubMed: 11576042]
11. Rogers ML, et al. Preliminary findings in the neurophysiological assessment of intercostal nerve injury during thoracotomy. Eur J Cardiothorac Surg. 2002; 21(2):298–301. [PubMed: 11825739]
12. Bruce J, et al. The prevalence of chronic chest and leg pain following cardiac surgery: a historical cohort study. Pain. 2003; 104(1-2):265–73. [PubMed: 12855337]
13. Sharma AD, et al. Peripheral nerve injuries during cardiac surgery: risk factors, diagnosis, prognosis, and prevention. Anesth Analg. 2000; 91(6):1358–69. [PubMed: 11093980]
14. Michaelson MD, et al. Management of complications of prostate cancer treatment. CA Cancer J Clin. 2008; 58(4):196–213. [PubMed: 18502900]
15. Walz J, Graefen M, Huland H. Basic principles of anatomy for optimal surgical treatment of prostate cancer. World J Urol. 2007; 25(1):31–8. [PubMed: 17333199]
16. Kehlet H, Jensen TS, Woolf CJ. Persistent postsurgical pain: risk factors and prevention. Lancet. 2006; 367(9522):1618–25. [PubMed: 16698416]
17. Peters TM. Image-guidance for surgical procedures. Phys Med Biol. 2006; 51(14):R505–40. [PubMed: 16825730]
18. Frangioni JV. In vivo near-infrared fluorescence imaging. Curr Opin Chem Biol. 2003; 7(5):626–34. [PubMed: 14580568]
19. Klohs J, Wunder A, Licha K. Near-infrared fluorescent probes for imaging vascular pathophysiology. Basic Res Cardiol. 2008; 103(2):144–51. [PubMed: 18324370]
20. De Grand AM, Frangioni JV. An operational near-infrared fluorescence imaging system prototype for large animal surgery. Technol Cancer Res Treat. 2003; 2(6):553–62. [PubMed: 14640766]
21. Gioux S, et al. Improved optical sub-systems for intraoperative near-infrared fluorescence imaging. SPIE Proceedings. 2005; 6009:39–48.
22. Gioux S, et al. High-power, computer-controlled, light-emitting diode-based light sources for fluorescence imaging and image-guided surgery. Mol Imaging. 2009; 8(3):156–65. [PubMed: 19723473]
23. Nakayama A, et al. Functional near-infrared fluorescence imaging for cardiac surgery and targeted gene therapy. Molecular Imaging. 2002:365–377. [PubMed: 12940233]
24. Tanaka E, et al. Image-guided oncologic surgery using invisible light: completed pre-clinical development for sentinel lymph node mapping. Ann Surg Oncol. 2006; 13(12):1671–81. [PubMed: 17009138]
25. Troyan SL, et al. The FLARE intraoperative near-infrared fluorescence imaging system: a first-in-human clinical trial in breast cancer sentinel lymph node mapping. Ann Surg Oncol. 2009; 16(10): 2943–52. [PubMed: 19582506]

26. Fagerholm U. The highly permeable blood-brain barrier: an evaluation of current opinions about brain uptake capacity. Drug Discov Today. 2007; 12(23-24):1076–82. [PubMed: 18061888]
27. Waterhouse RN. Determination of lipophilicity and its use as a predictor of blood-brain barrier penetration of molecular imaging agents. Mol Imaging Biol. 2003; 5(6):376–89. [PubMed: 14667492]
28. Stankoff B, et al. Imaging of CNS myelin by positron-emission tomography. Proc Natl Acad Sci U S A. 2006; 103(24):9304–9. [PubMed: 16754874]
29. Bos F. Optimization of spectral coverage in an eight-cell oscillator-amplifier dye laser pumped at 308 nm. Applied Optics. 1981; 20(20):3553–3556. [PubMed: 20372216]
30. Telle H, Huffer W. The XeCl Excimer Laser: A Powerful and Efficient UV Pumping Source for Tunable Dye Lasers. Optics Communications. 1981; 38(5,6):402–406.
31. Kluver H, Barrera E. A method for the combined staining of cells and fibers in the nervous system. J Neuropathol Exp Neurol. 1953; 12(4):400–3. [PubMed: 13097193]
32. Schmued L, Slikker W Jr. Black-gold: a simple, high-resolution histochemical label for normal and pathological myelin in brain tissue sections. Brain Res. 1999; 837(1-2):289–97. [PubMed: 10434014]
33. Stilwell DL. A sudan black B myelin stain for peripheral nerves. Stain Technol. 1957; 32(1):19–23. [PubMed: 13391323]
34. Wu C, et al. A novel fluorescent probe that is brain permeable and selectively binds to myelin. J Histochem Cytochem. 2006; 54(9):997–1004. [PubMed: 16709728]
35. Xiang Z, et al. Detection of myelination using a novel histological probe. J Histochem Cytochem. 2005; 53(12):1511–6. [PubMed: 16046669]
36. Schellingerhout D, et al. Fluorescence imaging of fast retrograde axonal transport in living animals. Mol Imaging. 2009; 8(6):319–29. [PubMed: 20003890]
37. Wu C, et al. Molecular probes for imaging myelinated white matter in CNS. J Med Chem. 2008; 51(21):6682–8. [PubMed: 18844339]
38. Gibbs-Strauss SL, et al. Molecular Imaging Agents Specific for the Annulus Fibrosus of the Intervertebral Disc. Molecular Imaging. 2009 in press.
39. Meyers JR, et al. Lighting up the senses: FM1-43 loading of sensory cells through nonselective ion channels. J Neurosci. 2003; 23(10):4054–65. [PubMed: 12764092]

A.

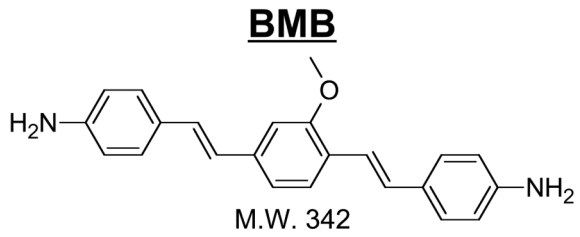

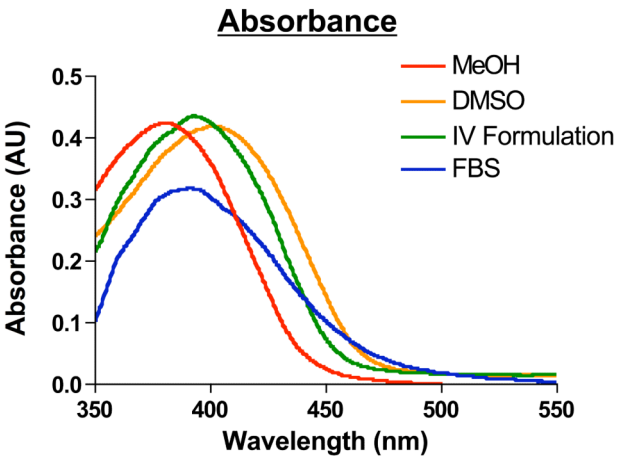

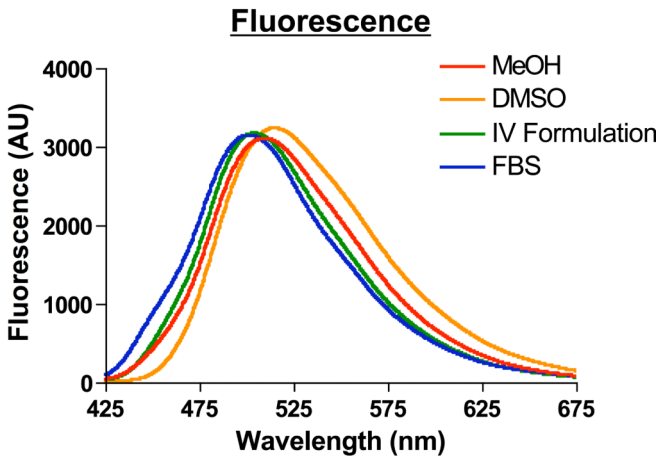

Condition	ε ($M^{-1}cm^{-1}$)	Ex Max (nm)	Em Max (nm)	QY (%)
DMSO	41,800	401	516	5.3
MeOH	42,300	382	510	4.7
FBS	34,300	390	501	2.3
IV Formulation	43,500	393	503	1.7

B.

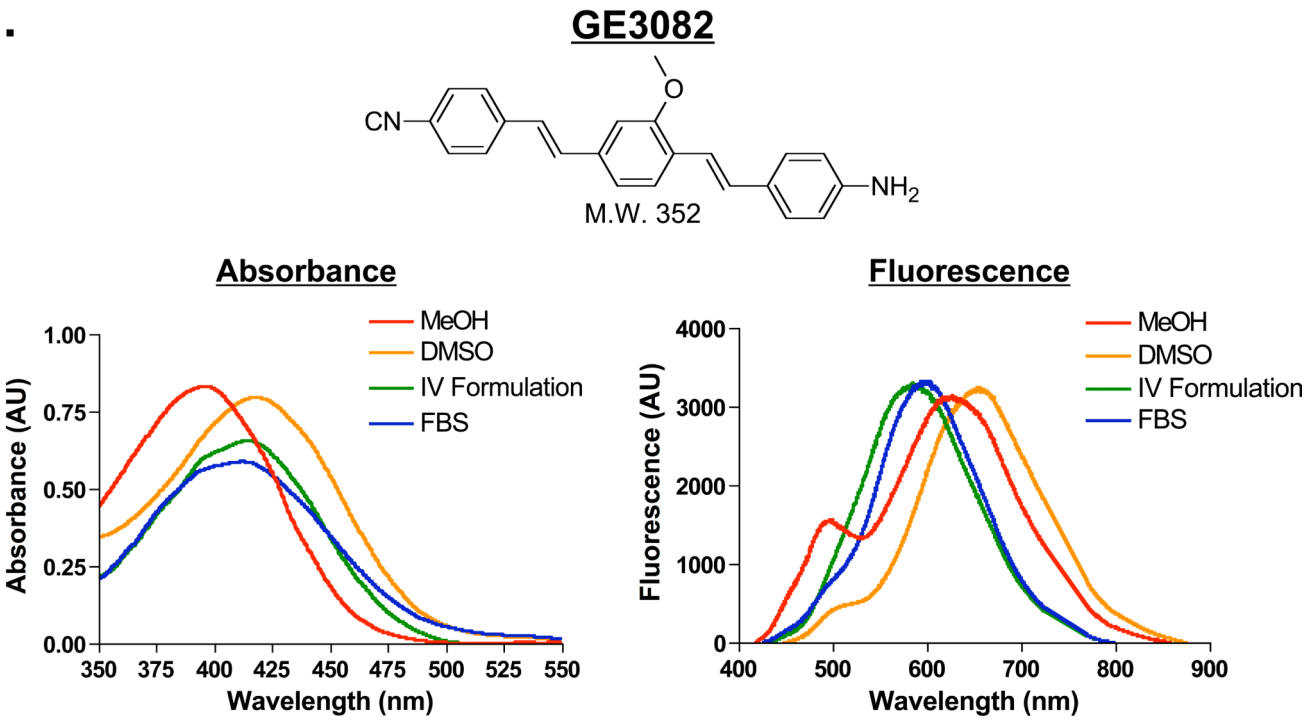

Condition	ε ($M^{-1}cm^{-1}$)	Ex Max (nm)	Em Max (nm)	QY (%)
DMSO	79,600	416	656	0.2
MeOH	83,200	396	628	0.07
FBS	58,900	411	599	1.7
IV Formulation	65,700	414	584	3.1

Figure 1. Structure and Spectral Properties of Fluorescent Nerve-Highlighting Agents

The chemical structure and molecule weight (top) for A) BMB and B) GE3082. The absorbance and fluorescence spectra in dimethyl sulfoxide (DMSO), absolute methanol (MeOH), the formulation used for IV administration (10% DMSO, 5% Cremophor, 65% serum, and 20% HEPES buffer), and fetal bovine serum buffered with 20 mM HEPES (FBS) (middle). The extinction coefficient, quantum yield, excitation and emission maximum in DMSO, MeOH, FBS and the IV Formulation (bottom).

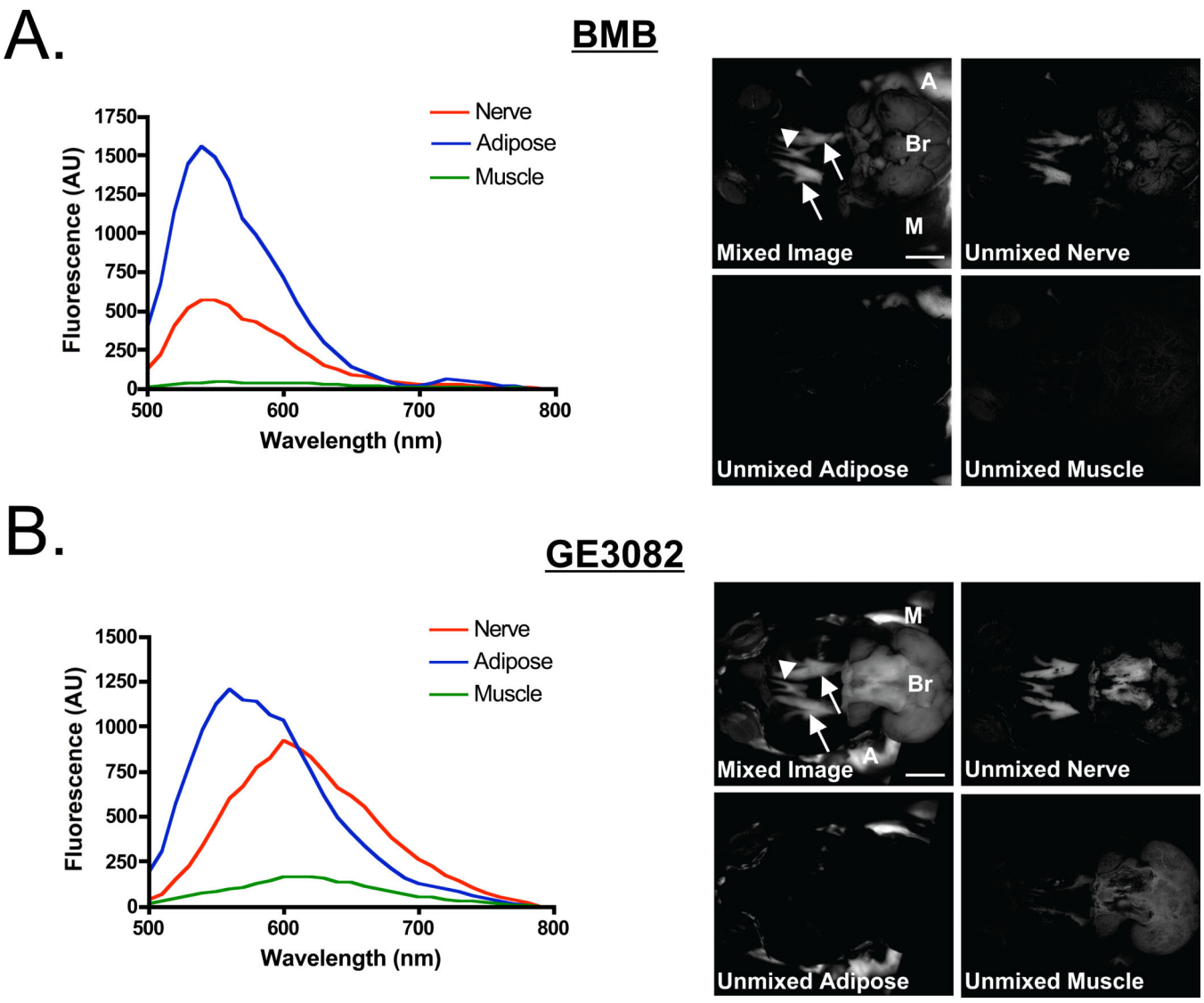

Figure 2. Spectral Properties of BMB and GE3082 *In Vivo*

In vivo fluorescence spectra 4 h after IV administration of 8.3 mg/kg (0.25 mg/mouse) of A) BMB and B) GE3082. Shown are the trigeminal ganglia (arrow), optic nerves (arrow head), brain (Br), adipose (A) and muscle (M) tissues. The spectrum of each tissue was unmixed from vehicle-injected control animal tissues (left). The original fluorescence image (mixed image) as well as unmixed nerve, adipose and muscle tissue images (right). Scale bar = 1 cm.

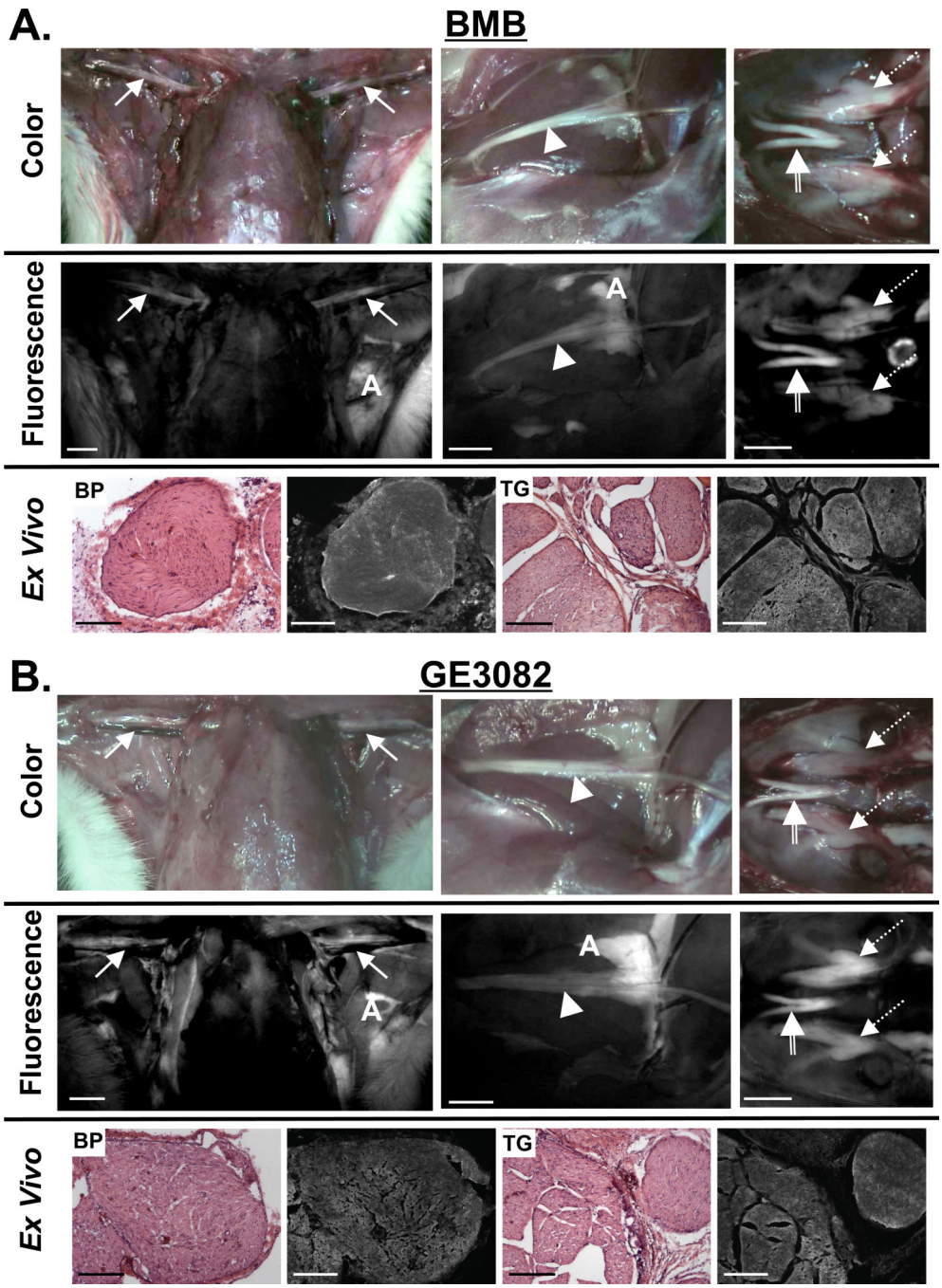

Figure 3. Image-Guided Surgery using Nerve-Specific Agents in Rats

Example nerve-to-muscle contrast for Sprague-Dawley rats administered 8.9 mg/kg A) BMB and B) GE3082. Shown are the brachial plexus (solid arrow), sciatic (arrowhead), trigeminal ganglia (dashed arrow) and optic nerves (striped arrow). Scale bars = 1 cm. A = adipose. *Ex vivo* microscopy images of the brachial plexus (BP) and trigeminal ganglia (TG) nerves serially sectioned for fluorescence microscopy and standard H&E microscopy. Scale bars = 200 μm.

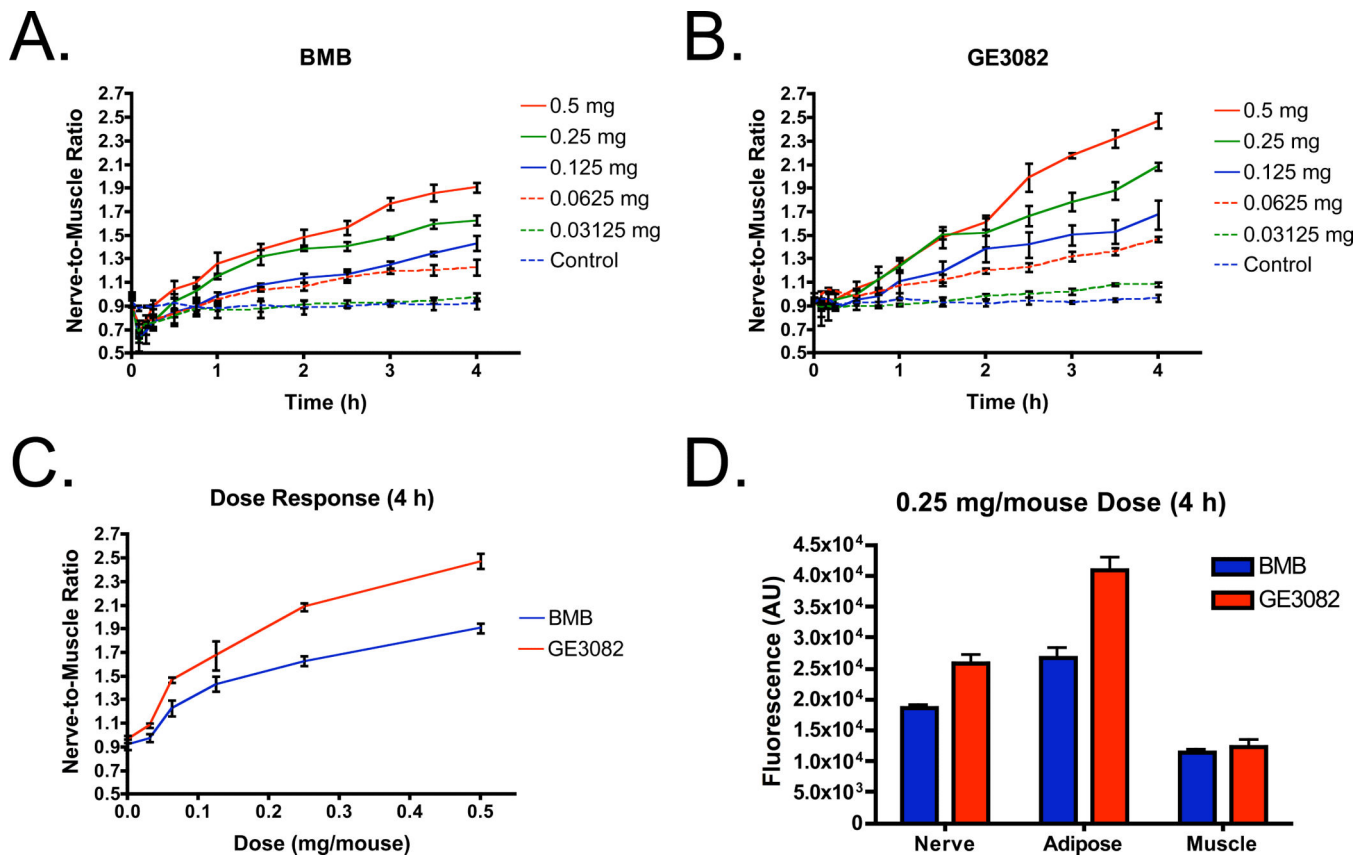

Figure 4. Kinetics, Dose and Tissue Specific Fluorescence

Kinetics of each fluorophore in mice following IV administration at serially-decreased doses from 0.5 mg/mouse (0.5, 0.25, 0.125, 0.0625 and 0.03125 mg/mouse and vehicle-injected control). Images were acquired prior to IV administration and at 5, 10, 15, 30, 45 and 60 min following administration of the fluorophore. Image acquisition continued every 30 min for up to 4 h. The nerve-to-muscle ratio (mean ± SD) of the brachial plexus to surrounding muscle tissue was calculated (n = 3 mice per group) for (A) BMB and (B) GE3082. (C) Nerve-to-muscle dose-response (mean ± SD) 4 h after IV administration. (D) Tissue specific fluorescence (mean ± SD) in the brachial plexus nerve, adipose and muscle tissue (n = 6 independent sites).

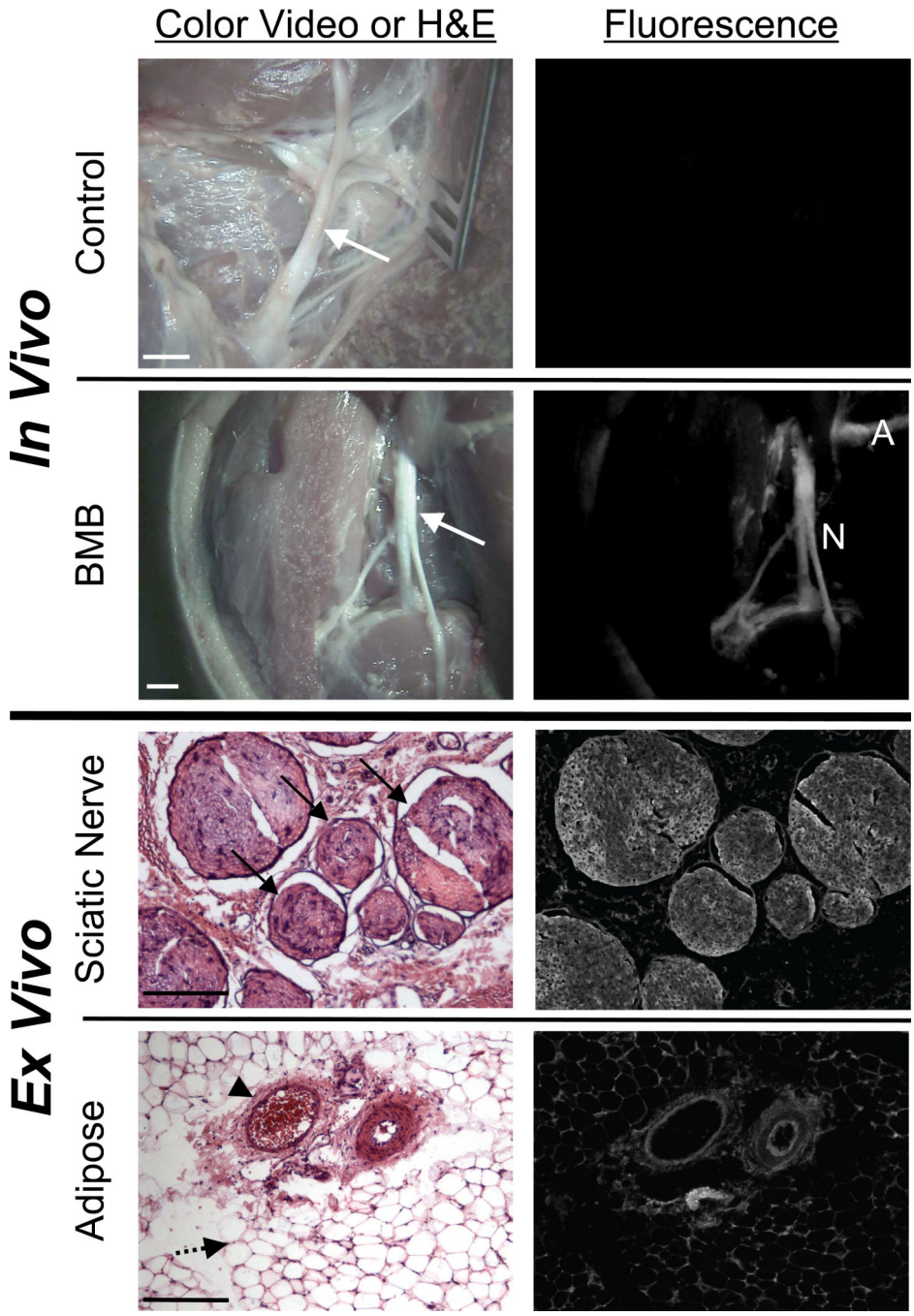

Figure 5. Real-Time Image-Guided Nerve Surgery in Pig using BMB

The sciatic nerves of Yorkshire pigs were imaged using the FLARE™ intraoperative imaging system.

A. The sciatic nerve (arrow) of a control pig in color video and fluorescence (top). The sciatic nerve (arrow) of a pig injected with 2.3 mg/kg BMB 8 h before imaging in color video and fluorescence (bottom), where adipose (A) and nerve (N) are highlighted. Scale bars = 1 cm. Data shown are representative of n = 5 independent experiments.

B. *Ex vivo* microscopy of pig sciatic nerve from (A) in cross-section (top) with visible nerve bundles (arrow) and adipose tissue (bottom) including blood vessels (arrow head) and adiposities (dashed arrow). Scale bars = 200 μm.

A.

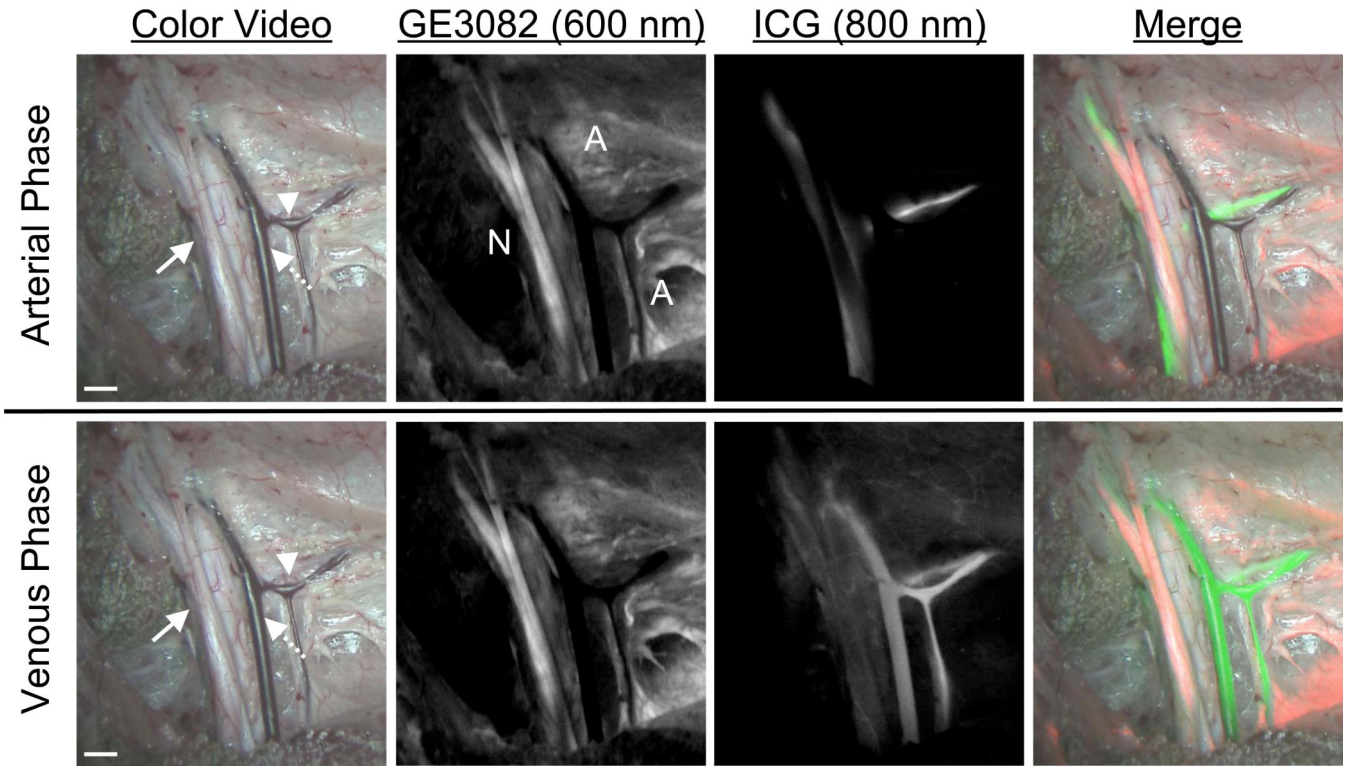

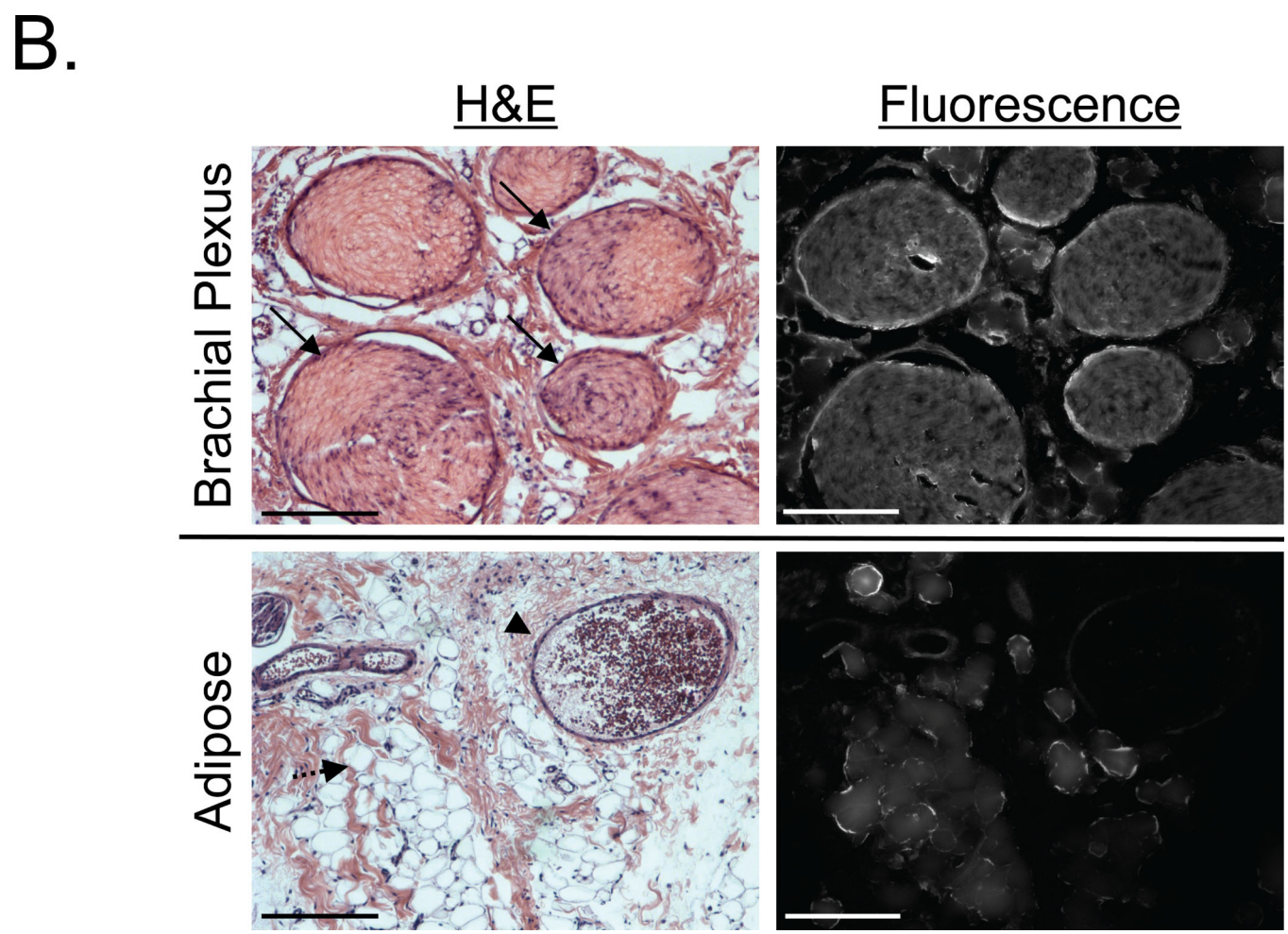

Figure 6. Simultaneous Imaging of Nerves and Blood Vessels during Pig Surgery using GE3082 and ICG

The brachial plexus nerves of Yorkshire pigs were imaged using the FLARE™ intraoperative imaging system.

A. Color video of the brachial plexus nerve (arrow), artery (arrowhead) and vessel (dashed arrow) of a pig 8 h after injection of 1.1 mg/kg GE3082 (top). The nerves and vessels were imaged simultaneously during the arterial (5 seconds after ICG administration, top row) and venous phases (2 minutes after ICG administration, bottom row). Nerve (N) and adipose (A) tissues were highlighted by GE3082 (column 2), vessels and arteries were highlighted by ICG (column 3), and a merged image of the color, GE3082 fluorescence (false-colored red), and ICG fluorescence (false-colored green) was displayed in real-time (column 4). Scale bars = 1 cm. Data shown are representative of n = 2 independent experiments.

B. *Ex vivo* microscopy of pig brachial plexus nerve from (A) in cross-section (top) with visible nerve bundles (arrow) and adipose tissue (bottom) including blood vessels (arrow head) and adiposities (dashed arrow). Scale bars = 200 μm.